Simulations of the Self-Focused Pseudospark-Sourced Electron Beam in a Background Ion Channel

LIANG ZHANG[ID], (Senior Member, IEEE), ALAN D. R. PHELPS[ID], (Member, IEEE), KEVIN RONALD, (Member, IEEE), AND ADRIAN W. CROSS, (Member, IEEE)
Department of Physics, Scottish Universities Physics Alliance (SUPA), University of Strathclyde, Glasgow G4 0NG, U.K.
Corresponding author: Liang Zhang (liang.zhang@strath.ac.uk)

ABSTRACT Using pseudospark discharge sourced electron beams for the generation of high-peak-power millimeter and terahertz radiation has attracted increasing research interest in recent years. However, one of the crucially important and hitherto unanswered questions is "what is the upper-frequency limit at which millimeter-wave devices can be driven by pseudospark discharge sourced electron beams?". In this paper, we studied this question from the perspective of beam transportation in a plasma background, more specifically an ion channel using particle-in-cell simulations to find the limitations. The parameter ranges of the beam transportation with small oscillations in the beam diameter were investigated and summarized, through simulations of beam propagation in a large diameter drift tube with different ion densities, plasma electron densities, beam density distributions, and beam energies. The beam transportation in a small diameter beam tunnel was also simulated. It showed the maximum beam current with a small velocity spread that can be transported in the beam tunnel was determined by the diameter of the beam tunnel and the ion density. High injected current will cause significant beam loss and reduce the overall efficiency. The simulation results indicate a minimum diameter of the beam tunnel in a millimeter-wave circuit that can be effectively driven by a pseudospark-sourced electron beam. The equivalent upper limit in the operating frequency is about 400 GHz.

INDEX TERMS Pseudospark discharge, PS-sourced beam, beam transportation, millimeter-wave source.

I. INTRODUCTION

Pseudospark (PS) discharges are low-pressure gas discharges in the range of 50 to 500 mTorr. The breakdown phase is rapid with the generation of a high current density electron beam up to 10^4 A/cm² [1]. The electron beam can be self-focused by the ion channel created by the ionization of the background gas, and propagate along a certain distance. These unique features have attracted many research interests for applications as high-current switches in high-power pulsed power systems, and as electron beam or plasma sources in lithography, material treatment and millimeter-wave generation [2]–[4].

The vacuum electronic device is the only practical solution for high-power, high-efficiency sub-millimeter wave generation [5]. As the operating frequency increases, the dimensions

The associate editor coordinating the review of this manuscript and approving it for publication was Shaoyong Zheng[ID].

of the interaction circuit, including the beam tunnel that has a cut-off frequency of the operating mode higher than the operating frequency are reduced. But at the same time the electron beam needs to be transported which results in the lowering of the overall beam current due to the decrease in the transverse cross-sectional area of the circuit. An electron beam with a high current density is therefore needed to maintain a high output power. However, the generation and transportation of the high-density electron beam in a small beam tunnel are one of the biggest challenges in the development of millimeter and sub-millimeter vacuum electronic devices. For example, a backward wave oscillator operating with a TM_{01} mode that has a cut-off frequency of 200 GHz has a mean radius of 0.57 mm [6]. The assembly and alignment of the focus magnet system and the electron gun required to form the electron beam become increasingly difficult to achieve. Research is being conducted on the use of sheet electron beams as they

have less space charge effect, enabling a current density that is ∼5 times higher than a cylindrical beam. However its focus magnet system is more complicated [7].

In recent years, there is growing interest in using the PS-sourced beam to drive slow-wave interaction circuits to generate millimeter and sub-millimeter wave radiation. Compared with the electron beam generated by a thermionic cathode, the PS-sourced beam has a current density ∼100 times larger. Therefore it has the advantage to generate high output power radiation at millimeter and sub-millimeter wavelengths. The PS-sourced beam is self-focused by the ion channel that it creates through ionizing the background gas. This eliminates the need for a bulky magnet system. Since the electron beam is generated from a plasma cathode, it has the advantage to generate electron beams with different cross-sections, including cylindrical and sheet geometries, to match with different types of interaction circuits, such as the Cherenkov maser, the backward wave oscillator, and the extended interaction oscillator (EIOs) [6], [8]–[11]. Different beam properties can also be achieved by varying the discharge conditions. Electron beams with different energies can be produced by adjusting the charging voltage and the gap distance across the cathode and the anode. The pulse duration can be adjusted in a certain range by using different external capacitors which store the energy for the gas discharge. The higher capacitance will result in longer pulse duration and higher discharge current. The peak discharge current is also strongly associated with the geometry of the discharge chamber. A more detailed description of the experimental setup for the PS discharge can be referred to in [11]–[14].

In our previous research, EIOs driven by PS-sourced beams have been designed and measured experimentally at different frequencies [12], [14]. In the experiment, it was found that the output radiation power dropped much faster than simulations predicted at higher operating frequencies. To match with the measurement results, either the beam current must be significantly reduced, or the beam quality must be much worse in the interaction circuit. Although the overall beam current as a function of the propagation distance can be measured by a Faraday cup, it cannot provide information on the beam quality in terms of beam energy spread and velocity spread, which are critical beam parameters that affect the beam-wave resonance condition. As for the application of millimeter vacuum electron devices, the beam measurements in the interaction circuit become increasingly difficult due to the small radius of the beam tunnel (less than 1 mm) which limits the size of the probes.

Numerical simulation is an effective method to get the dynamic information of the beam transportation in the plasma background within the beam-wave interaction circuit. In this paper, the theoretical model is first summarized to get the conditions of stable transportation of the electron beam in a plasma background. The particle-in-cell (PIC) simulations were then used to further explore the parameter ranges that allow stable beam transportation, firstly in a drift tube with a large diameter, then in a beam tunnel of the beam-wave
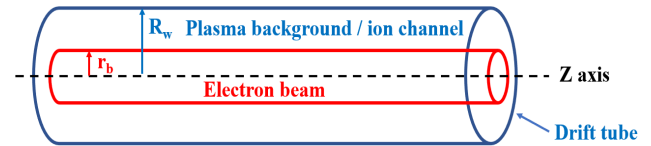

FIGURE 1. A schematic drawing of the electron beam transported in a plasma background.

interaction circuit. The potential and the limits of using the PS-sourced beam to drive the THz vacuum electronic devices are also discussed.

II. BRIEF SUMMARY OF THE THEORETICAL MODEL FOR BEAM TRANSPORTATION IN PLASMA BACKGROUND

When an electron beam transports in a low-pressure gas, its beam front will ionize the background gas to create a plasma background [15], [16]. The plasma electrons have larger velocities than the ions. They will be expelled by the beam electrons to leave an ion channel. The ion channel contains a net positive charge, which provides a focusing force to neutralize the space charge force from the beam electrons [17].

The theoretical study of the relativistic electron beam transportation in the ion channel has been derived in detail in [18] based on the equilibrium analysis. Here only the key concepts and conclusions are summarized. Fig. 1 shows the general schematic of the theoretical model. A cylindrical electron beam with a radius of r_b travels along the z coordinate with a velocity of v_{bz}. The drift tube has a radius of R_w. The Gauss' and Ampere's laws in the plasma background at the steady state in cylindrical coordinates can be written in (1), where cgs units are used for convenience.

$$\begin{cases} \dfrac{1}{r}\dfrac{\partial}{\partial r}r\dfrac{\partial \Phi}{\partial r} = -4\pi e(n_i(r) - n_e(r) - n_{b0}(r)) \\ \dfrac{1}{r}\dfrac{\partial}{\partial r}r\dfrac{\partial A_z}{\partial r} = \dfrac{4\pi}{c}en_{b0}(r)\cdot v_{bz}(r)\cdot(1 - f_m) \end{cases} \quad (1)$$

The parameters Φ, and A_z are the potentials of the electric and magnetic fields, respectively. n_{b0}, n_i, n_e, and v_{bz} are the beam electron density, ion density, trapped plasma electron density, and the electron beam axial velocity, respectively. f_m is the current neutralization fraction. Let $f_b = n_{b0}/n_i$ as the charge neutralization fraction, and $f_e = n_e/n_i$ as the fraction of trapped plasma electrons, when $f_e = 1 - f_b$, the system maintains charge neutrality. As the trapped plasma electrons in the drift tube will interact with the electron beam to cause a two-stream instability [19]–[21], the number of trapped electrons should be minimized. which requires $1 - f_b \approx 0$.

Another requirement on the ion and beam densities associates with the betatron oscillation, the betatron frequency can be written as

$$\Omega_\beta^2 = \frac{\omega_{pb}^2}{2\gamma_0}\left(\frac{1}{f_b} - [1 - \beta^2]\right) \quad (2)$$

where $\omega_{pb} = (4\pi n_{b0}e^2/m_e)^{1/2}$ is the plasma frequency of the electron beam in cgs units. $\beta = v_{bz}/c$, and c is the speed of
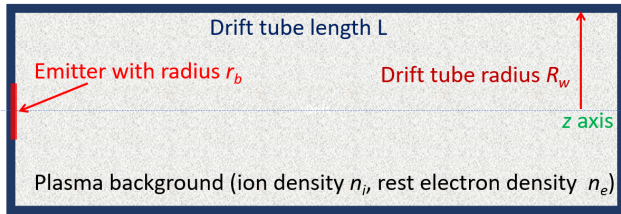
FIGURE 2. The simulated model in XOOPIC.

light. e and m_e are the electron charge and mass, respectively. In a practical system, $\Omega_\beta^2 > 0$ is required. Therefore, to focus the electron beam at both axial and radial directions, both $f_b < \gamma_0^2$ and $1 - f_b \approx 0$ need to be satisfied.

III. PIC SIMULATION MODEL

The theory presented in the previous section is useful to describe the physical processes governing the relativistic electron beam transportation in a plasma background, in particular the mathematical description of the ion channel. However the equilibrium analysis has a few assumptions. One of them is $v/\gamma \ll 1$ which is more applicable for high energy electron beams used for accelerator applications. Here $v = I_b/(I_A\beta)$ is the Budker parameter, where I_b is the beam current, and I_A is the Alfven current. It may not be valid for the PS-sourced beam due to the low beam energy and high PS discharge current. Also the conditions $f_b < \gamma_0^2$ and $1 - f_b \approx 0$ are too rough. The PIC simulations can provide detailed beam dynamics and were used in the study of electron beam parameters in more detail than could be achieved by analytical techniques.

The simulation model is shown in Fig. 2. The PS discharge process was not included due to the large volume of the discharge cavity compared with the drift tube. Normally the diameter of the discharge cavity is ∼10 times larger than that of the drift tube, which will significantly increase the computing time. Also for this gas discharging problem, the potential on the external charging capacitor needs to be solved for every time step to reflect the real experimental configuration. The parallel computing feature cannot be applied [13]. The simulation was carried out in cylindrical coordinates using XOOPIC [22]. The simulation region is a cylinder tube with a perfect electric conductor (PEC) boundary representing the drift tube. The left end represents the anode of the pseudospark discharge chamber, where an emitter with a radius r_b shows the aperture size of the central hole in the anode where the electron beam is extracted. The electron beam was injected from the left-hand side of the drift tube and transported to the right-hand side. The conductor at the right-hand side is the collector to dump the electron beam. The length of the drift tube L was 200 mm in the simulation.

Simplified models were used to speed up the simulation and focus on the major physics phenomena. The collisions between the injected electrons and the background gas were ignored. The ionization process is also ignored to avoid the rapid growth of the simulated particle number. Instead, the

plasma background was pre-set and filled in the drift tube. It is reasonable because the PS discharge contains three breakdown stages, the Townsend discharge (pre-breakdown) stage, the hollow-cathode discharge stage, and the super-dense glow discharge stage [23]. The Townsend discharge has a low beam current and a long duration. The plasma background is created prior to the electron beam generated in the hollow-cathode discharge stage, which has a balanced performance of beam energy and current for beam-wave interaction. The plasma density at the hollow-cathode discharge stage is in the range of 10^{16} m^{-3} to 10^{18} m^{-3}. XOOPIC employs a time-explicit scheme. The mesh grids in the simulations were 20 μm and 50 μm in the radial and axial directions, respectively. The time step was 1×10^{-13} s to meet the Courant condition. The numerical weight of the macro-particles was 1×10^3. The simulations were run on a PC running the Debian operating system. The CPU was an Intel i9-7900X at 3.3 GHz, and with 64 GB RAM. The computing time for each simulation was about 2 hours. The simulation time can be a factor of 5 longer if the ionization process is included since more particles will exist in the simulation region.

The beam transportation at different plasma densities was simulated. The phase space of the particles as well as the density information of the ions and the electrons were recorded every 50 timesteps for further post-processing. The results are shown in the following sections.

IV. SIMULATION RESULTS
A. PHASE SPACE OF THE ELECTRON BEAM AT DIFFERENT BEAM CURRENTS

In the simulations, the beam radius was 1.5 mm which matches with the 3-mm diameter aperture on the anode used in the experiment. The beam energy was 5 keV corresponding to a single-gap PS-discharge configuration [24], [25]. Different beam currents that represent different electron densities were used in the simulations. A drift tube with a radius of 5.0 mm and a length of 200 mm was used, which allows the observation of the beam transportation without striking on the wall of the drift tube. The ion density n_i was set as 1×10^{17} m^{-3}, and the plasma electron density n_e was set as 1×10^{14} m^{-3} (0.1% of the ion density to avoid the two-beam instability.).

Fig. 3 shows the phase space of the injected beam with uniform distribution propagating at different electron beam currents, (a) 0.94 A, (b) 4.23 A, and (c) 14.1 A, which are equivalent to beam density n_{b0} of 0.2×10^{17} m^{-3}, 1.0×10^{17} m^{-3} and 3.24×10^{17} m^{-3}. A small current electron beam whose density is smaller than the ion density will be over-focused. Because of the difference in the space charge at different radius, the laminarity of the electron beam becomes worse and the electrons will cross with each other (Fig. 3(a)). A similar trend happens when the beam current is too large, the ion channel is not able to provide sufficient focusing force and the beam envelope will expand gradually (Fig. 3(c)). The best beam quality with a small ripple and a good laminarity can be achieved, as shown in Fig. 3(b), when $f_b \approx 1$,
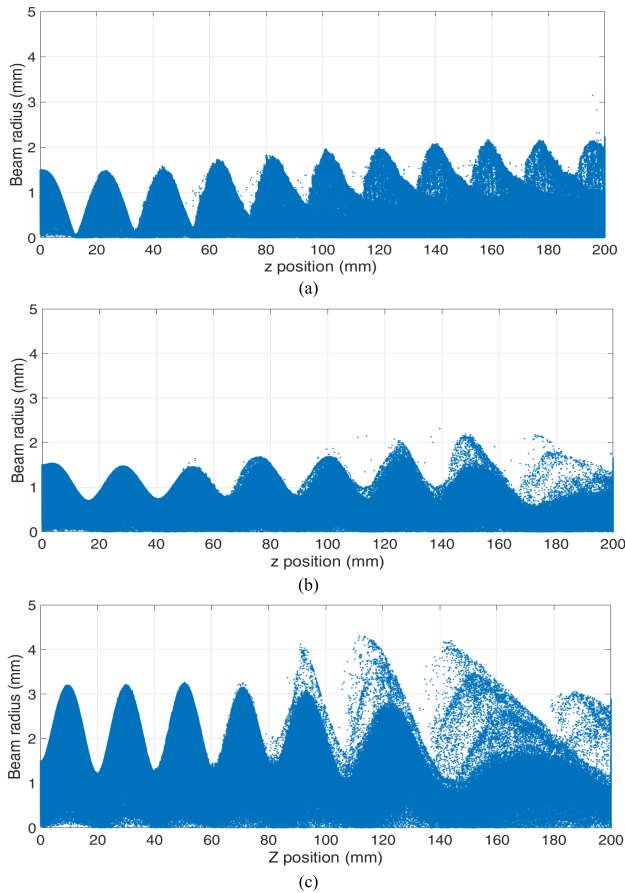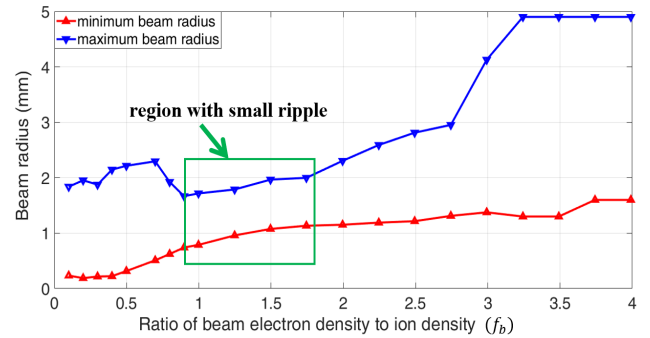
FIGURE 3. PIC phase space of the electron beam with different densities transporting in an ion channel with fixed ion density n_i of 1.0×10^{17} m^{-3}. The beam density n_{b0} is (a) 0.2×10^{17} m^{-3}, (b) 1.0×10^{17} m^{-3}, (c) 3.24×10^{17} m^{-3}.

FIGURE 4. The maximum and minimum beam radii at different f_b.

FIGURE 5. The maximum and minimum beam radii as the function of f_b at different ion densities.

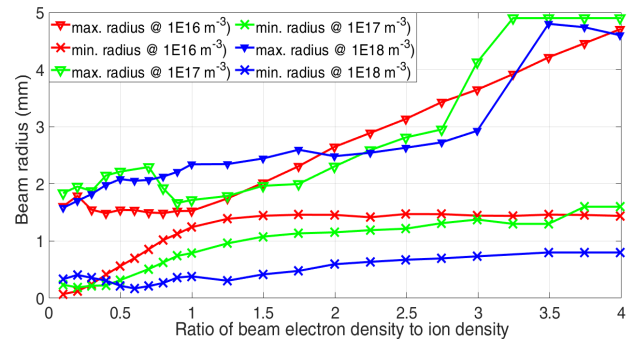corresponding to the charge neutrality and from the theory a small $f_e \approx 0.1\%$ was used.

The phase space of emitted electrons was post-processed to get its envelope during the transportation. The maximum and minimum radii on the envelope were recorded to quantify the beam quality. Fig. 4 shows the maximum and minimum radii of the beam envelope which were post-processed from the phase space of the beam electrons. It shows the parameter region where a small ripple can be achieved, which is desired for the beam-wave interaction to generate millimeter-wave radiation. In general, the minimum radius increases as the beam density increases because the space charge force becomes larger. The maximum beam radius occurred when $f_b = 1$. In the case of $f_b > 2.5$ that the electron beam defocused significantly, the electron beam envelope expands rapidly and strikes the wall of the drift tube.

B. THE RESULTS AT DIFFERENT ION DENSITIES, BEAM ENERGIES, AND CURRENT DENSITY DISTRIBUTIONS

The plasma density during the PS discharge process changes dynamically at different stages, from 10^{13}-10^{14} m^{-3} at the Townsend discharge stage, 10^{16}-10^{18} m^{-3} at the hollow-cathode discharge stage, to 10^{20} m^{-3} at the

super-dense glow discharge stage [13]. The beam transportation at different ion densities in the hollow-cathode discharge stage was also simulated and the results are shown in Fig. 5. Similar trends with Fig. 4 can be observed. A small beam density n_{b0}, for example below 10^{17} m^{-3}, the f_b range with a small ripple suggested by Fig. 4 is still valid which falls within the range from 0.8 to 1.8. At a low plasma density, the beam current is low and the space charge is small. The electron beam can be effectively focused. As the plasma density increases, the space charge of the beam electrons becomes large which increases the fluctuation. Although the overall beam current increases, the poorer beam quality will reduce the beam-wave interaction efficiency. This implies that in this case, a high plasma density or equivalently a high beam current is undesired, for generating millimeter-wave radiation.

The PS discharge can be used to generate electron beams with different energies, depending on its configuration. The single-gap configuration has a limit of charge voltage ~20 kV due to the flashover at the dielectric insulator, as well as the electric field uniformity on a long dielectric tube. The multi-gap configuration can increase the charging voltage and therefore generate a high-energy beam [26]. To make a compact millimeter-wave device, the energy of the PS-sourced beam is normally ~30 keV or lower, depending on the types of interaction circuits.

Fig. 6 shows the results at different beam energies. At higher beam energy, the space charge force is small
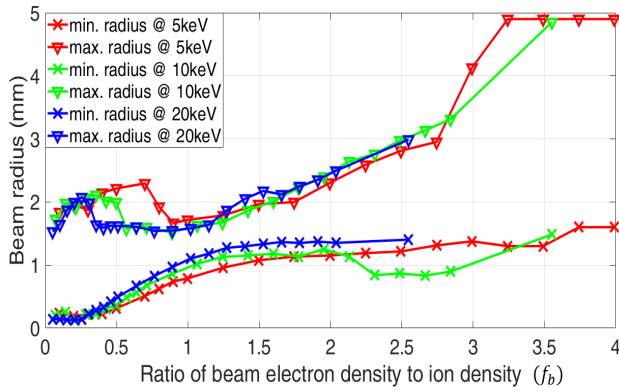
FIGURE 6. The maximum and minimum beam radii as the function of $f_b(n_i = 10^{17} \text{ m}^{-3})$ at different beam energies.

and the electron beam can have a small ripple. The f_b range with a small ripple is larger when the beam energy increases.

The theoretical analysis and the previous simulations employed uniform electron beam density distribution profiles over the beam radius. However, the electron beam density measurement using a scintillator screen showed that the PS-sourced beam has a Gaussian-like density distribution and a beam waist of 0.5 mm [27]. The injected electron beam used was of the same overall current but different density distributions. Fig. 7 shows the current distributions as well as the minimum and maximum beam radii for all the cases at a beam energy of 5 keV, and an ion density of 10^{17} m^{-3}. In the post-processing, the average beam density was used to calculate f_b. At the Gaussian distribution with a smaller beam size, the beam ripple is smaller when it is over-focused because the space-charge force is smaller at a larger radius.

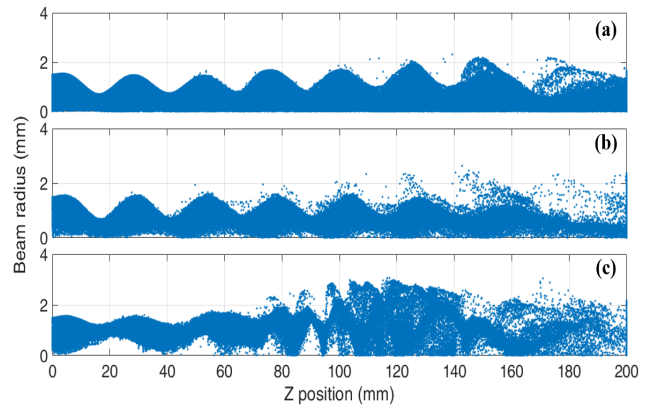### C. IMPACT OF TRAPPED PLASMA ELECTRONS

The simulation results in the previous section show the electron beam can be transported a long distance with small losses over a wide parameter range if the diameter of the drift tube is large. A small ripple in the electron beam envelop can be achieved for the conditions:

$$\begin{cases} H \geq 10 \text{ keV} \\ n_i \leq 10^{17} \text{ m}^{-3} \\ f_b \in [0.81.8] \end{cases} \quad (3)$$

As has been mentioned in the previous sections, the trapped plasma electrons may cause two-stream instability. Fig. 8 shows the phase space of the beam electrons at different f_e levels. When the trapped plasma electron density is small, for example, $f_e = 1\%$ then only a small oscillation close to the z-axis is observed. The distortion on the electron beam is relatively small. However as the value of f_e increases, the beam transportation becomes unstable. The electron beam starts to oscillate initially at larger z positions and then the beam transportation is destroyed, as shown in Fig. 8(c) when $f_e = 10\%$. The electron beam desired in a vacuum electronic
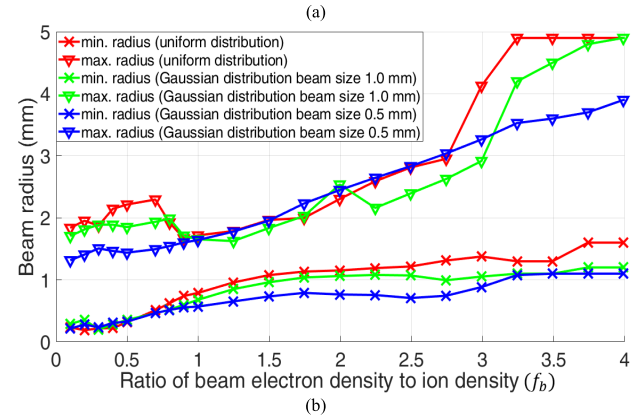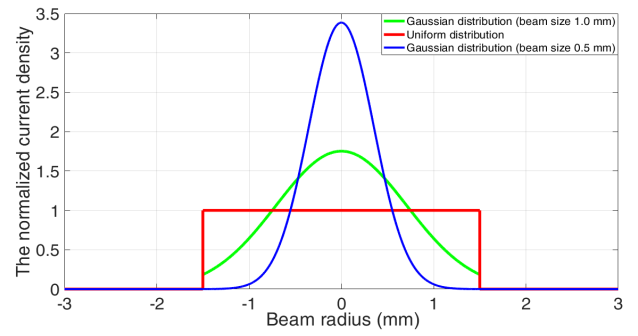
FIGURE 7. (a) The different current density distributions, (b) The maximum and minimum beam radii as the function of $f_b(n_i = 10^{17} \text{ m}^{-3})$ at different current density distributions.

FIGURE 8. Phase space of the beam electrons at different levels of trapped plasma electrons. (a) $f_e = 0.1\%$, (b) $f_e = 1\%$, (c) $f_e = 10\%$.

device will have a small ripple and good laminarity. Therefore the trapped plasma electron density needs to be as small as possible to avoid the betatron oscillation.

### V. PS-SOURCED BEAM TRANSPORTATION IN A SMALL BEAM TUNNEL

In the simulations presented in previous sections, the electron beam is propagated in a drift tube with a large diameter and the electron beam can propagate a long distance before it strikes the wall of the drift tube. In the application of millimeter-wave devices, the dimension of the drift tube

is limited by the operating frequency since it will need to cut off the radiation wave. The smallest radius dictates the maximum frequency that can realistically be generated by the millimeter-wave device. The beam transportation in the small drift tube (beam tunnel) is studied in this section. So far the PS-sourced beam has been used for the linear-beam vacuum electronic devices which employ the TM-like mode. When the radius of the beam tunnel is 0.5 mm, the cut-off frequency of the lowest mode TM_{01} is 229.5 GHz. Since the beam tunnel needs to cut off the operating mode of the interaction circuit to stop the electromagnetic wave from propagating to the electron beam source, the operating frequency of the interaction circuit should be lower than this cut-off frequency. Operating at a higher frequency requires a smaller radius of the beam tunnel. At the same time, it is preferred that the beam tunnel has a larger radius for containing a higher electron current to achieve a higher output power. As a trade-off, the optimal operating frequency range of the interaction circuit with a beam tunnel of 0.5 mm is around 200 GHz. The length of the beam tunnel is chosen as 50 mm which is sufficient for most types of the interaction circuit.

The electron beam used in the simulation has a Gaussian density profile and the beam size is 0.5 mm. At a small drift tube radius, part of the beam current will be lost at the wall of the tunnel. It is important to know the percentage of the beam lost. In the simulation, the small ripple parameter regime, as summarized in Eqn. 3, was used. The parameters used were $H = 20$ keV, $n_i = 10^{17}$ m^{-3}, and $f_e = 0.1\%$. The beam current and velocity spread are two important parameters when considering an electron beam used to drive the interaction circuit of the millimeter-wave devices.

Fig. 9(a) shows the beam current and Fig. 9(b) shows the beam velocity and its spread as errorbars, as the function of the transportation distance at different f_b values. The simulation shows under a limited radius of the beam tunnel, the beam can transport over a short distance ($\sim$5 mm) without large beam loss, because the beam current is relatively high but the space charge needs time to take effect. Then a big current loss can happen during the propagation and finally, the beam current becomes stable as the result of the re-balance of the space charge force and the focusing force provided by the ion channel. The larger the input current, the greater the beam loss. Fig. 9(a) also indicates a maximum beam current that can be transported in the beam tunnel of radius 0.5 mm, in this case is 0.53 A, with small beam loss and small energy spread. A high injected current does not turn into a high transmitted current. Fig. 9(b) shows the velocity spread of the beam at different transportation distances. The velocity spread is relatively small during the transportation to keep a good beam quality, and a higher injected current will have a slightly higher velocity spread.

In the case of a small beam tunnel, the trapped plasma electrons have less impact on the beam transportation, as they
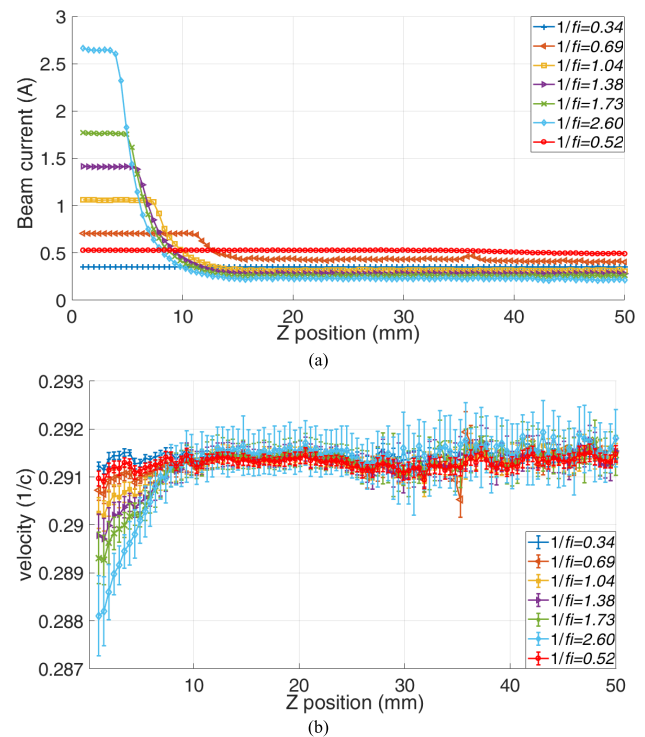
FIGURE 9. (a) The beam current, and (b) the velocity spread of the electron beam as a function of propagation length at different $f_b(n_i = 10^{17}$ m^{-3}).
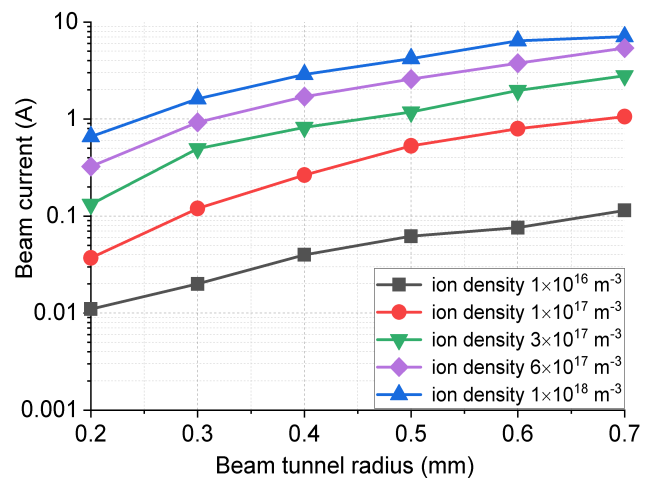
FIGURE 10. The maximum beam current allowed at different beam tunnel radii and ion densities.

are much easier to be expelled by the beam electrons and collected by the wall of the beam tunnel. The optimal beam current does not change even with an f_e factor of up to 20%, while the velocity spread will increase by about 2%.

The maximum current in the beam tunnel at different radii of the beam tunnel and the ion densities are shown in Fig. 10. The maximum current increases rapidly when the beam tunnel radius increases, which shows the PS-beam can be an effective beam source at a lower frequency. For example, consider an interaction circuit operating with a

TM_{01} mode, the cut-off frequency for a radius of 0.7 mm is 163.9 GHz, which enables 1.0 A of self-focused beam current to be transported in the beam tunnel under the ion density of 10^{17} m^{-3}. Higher ion density allows a larger beam current. However in the simulation, it showed the velocity increases rapidly when the ion density gets close to 10^{18} m^{-3}. Operating at an ion density around 10^{17} m^{-3} is preferred as the balance point between beam current and the beam quality. If an interaction circuit is operating with a TM_{01} mode and a beam tunnel radius of 0.29 mm, corresponding to a cut-off frequency of 400 GHz, then the maximum beam current is ~0.1 A, it is then difficult to satisfy the starting current condition taking into consideration the high ohmic loss at high frequency [28].

VI. DISCUSSION AND CONCLUSION

A PS-sourced beam has the unique advantages of high current density and self-focus by the ion channel. In the past 10 years, experiments have been carried out to use a PS-sourced beam to drive the slow-wave interaction circuit to generate microwave and millimeter-wave radiation. Due to the challenges of generation and transportation of the high current beams in the millimeter/submillimeter-wave vacuum electronic devices, there is increasing research interest in the PS-sourced beam to drive the interaction circuit at a higher frequency. Compared with the millimeter/submillimeter-wave vacuum electronic devices driven by an electron beam generated from a thermionic gun, the PS-source electron beam has a much higher current density, therefore allowing millimeter/submillimeter-wave radiation to be generated with higher peak power. However, the previous experiments also showed that the output radiation power drops as the operating frequency increases. Therefore, it is important to know the limit of the operating frequency.

In contrast to the research work on designing the submillimeter-wave interaction circuit driven by a PS-beam, this paper first investigates the general case of a PS-sourced electron beam transportation in a plasma background to study the parameter range for smooth transportation. The desired parameter range, as listed in Eqn. 3 was summarized from various PIC simulations. This indicates the PS-sourced beam can keep a relatively good quality if all the conditions are met, which is feasible to achieve by adjusting the experimental conditions.

The simulations show when limited by the dimensions of the beam tunnel, there exists an optimal injected current. A higher injected current will result in a larger beam loss although the velocity spread is relatively low. This is not desirable for millimeter-wave devices, as it will significantly reduce the overall efficiency. As the operating frequency of the millimeter-wave device increases, the dimensions of the beam tunnel reduces and it will further limit the maximum current that can be transported in the beam tunnel. On the other hand, the ohmic loss of the interaction circuit becomes higher at a higher frequency to make the starting current higher, which can be ~0.4 A, depending on the geometric

shunt impedance (R/Q) of the interaction circuit and its beam loading conductance.

The limit of the maximum injected current not only dramatically reduces the output power, but also can stop the device from working due to the high starting current requirements. Based on the beam transportation simulations for different beam tunnel diameters and the experience of the high-frequency interaction circuits, it is estimated that the upper limit of the millimeter-wave devices driven by a PS-sourced beam is 400 GHz. It is possible to increase the beam current by operating at higher ion density, however the beam quality will get worse making the device hard to operate stably and reliably.

REFERENCES

[1] J. Christiansen and C. Schultheiss, "Production of high current particle beams by low pressure spark discharges," *Zeitschrift Phys. A Atoms Nuclei*, vol. 290, no. 1, pp. 35–41, Mar. 1979, doi: 10.1007/bf01408477.

[2] S. V. Lebedev, M. Machida, S. A. Moshkalyov, and D. O. Campos, "Experimental study of the pseudospark-produced electron beam for material processing," *IEEE Trans. Plasma Sci.*, vol. 25, no. 4, pp. 754–757, Aug. 1997, doi: 10.1109/27.640699.

[3] C. Jiang, A. Kuthi, M. A. Gundersen, and W. Hartmann, "Pseudospark electron beam as an excitation source for extreme ultraviolet generation," *Appl. Phys. Lett.*, vol. 87, no. 13, Sep. 2005, Art. no. 131501, doi: 10.1063/1.2053352.

[4] D. Bowes, H. Yin, W. He, L. Zhang, A. W. Cross, K. Ronald, A. D. R. Phelps, D. Chen, P. Zhang, X. Chen, and D. Li, "X-ray emission as a diagnostic from pseudospark-sourced electron beams," *Nucl. Instrum. Methods Phys. Res. B, Beam Interact. Mater. Atoms*, vol. 335, pp. 74–77, Sep. 2014, doi: 10.1016/j.nimb.2014.06.008.

[5] S. S. Dhillon, M. S. Vitiello, E. H. Linfield, A. G. Davies, M. C. Hoffmann, J. Booske, C. Paoloni, M. Gensch, P. Weightman, G. P. Williams, and E. Castro-Camus, "The 2017 terahertz science and technology roadmap," *J. Phys. D, Appl. Phys.*, vol. 50, no. 4, Feb. 2017, Art. no. 043001, doi: 10.1088/1361-6463/50/4/043001.

[6] W. He, L. Zhang, D. Bowes, H. Yin, K. Ronald, A. D. R. Phelps, and A. W. Cross, "Generation of broadband terahertz radiation using a backward wave oscillator and pseudospark-sourced electron beam," *Appl. Phys. Lett.*, vol. 107, no. 13, Sep. 2015, Art. no. 133501, doi: 10.1063/1.4932099.

[7] J. P. Pasour, E. Wright, K. T. Nguyen, A. Balkcum, F. N. Wood, R. E. Myers, and B. Levush, "Demonstration of a multikilowatt, solenoidally focused sheet beam amplifier at 94 GHz," *IEEE Trans. Electron Devices*, vol. 61, no. 6, pp. 1630–1636, Jun. 2014, doi: 10.1109/TED.2013.2295771.

[8] N. Kumar, R. P. Lamba, A. M. Hossain, U. N. Pal, A. D. R. Phelps, and R. Prakash, "A tapered multi-gap multi-aperture pseudospark-sourced electron gun based X-band slow wave oscillator," *Appl. Phys. Lett.*, vol. 111, no. 21, 2017, Art. no. 213502, doi: 10.1063/1.5004227.

[9] A. W. Cross, H. Yin, W. He, K. Ronald, A. D. R. Phelps, and L. C. Pitchford, "Generation and application of pseudospark-sourced electron beams," *J. Phys. D, Appl. Phys.*, vol. 40, no. 7, p. 1953, 2007.

[10] G. X. Shu, H. Yin, L. Zhang, J. P. Zhao, G. Liu, A. D. R. Phelps, A. W. Cross, and W. He, "Demonstration of a planar W-band, kW-level extended interaction oscillator based on a pseudospark-sourced sheet electron beam," *IEEE Electron Device Lett.*, vol. 39, no. 3, pp. 432–435, Mar. 2018, doi: 10.1109/led.2018.2794469.

[11] G. X. Shu, L. Zhang, H. Yin, J. P. Zhao, A. D. R. Phelps, A. W. Cross, G. Liu, Y. Luo, Z. F. Qian, and W. He, "Experimental demonstration of a terahertz extended interaction oscillator driven by a pseudospark-sourced sheet electron beam," *Appl. Phys. Lett.*, vol. 112, no. 3, Jan. 2018, Art. no. 033504, doi: 10.1063/1.5011102.

[12] G. Shu, W. He, L. Zhang, H. Yin, J. Zhao, A. W. Cross, and A. D. R. Phelps, "Study of a 0.2-THz extended interaction oscillator driven by a pseudospark-sourced sheet electron beam," *IEEE Trans. Electron Devices*, vol. 63, no. 12, pp. 4955–4960, Dec. 2016, doi: 10.1109/ted.2016.2615314.

[13] L. Zhang, W. He, X. Chen, J. Zhang, and A. W. Cross, "Characteristics of pseudospark discharge in particle-in-cell simulations," *IEEE Trans. Electron Devices*, vol. 68, no. 6, pp. 3003–3009, Jun. 2021, doi: 10.1109/TED.2021.3073877.

[14] J. Zhao, H. Yin, L. Zhang, W. He, Q. Zhang, A. D. R. Phelps, and A. W. Cross, "Experiments on W-band extended interaction oscillator with pseudospark sourced post-accelerated electron beam," *Phys. Plasmas*, vol. 24, no. 6, Jun. 2017, Art. no. 060703, doi: 10.1063/1.4985684.

[15] U. N. Pal, P. Shukla, A. S. Jadon, and N. Kumar, "Estimation of beam and plasma parameters for electron beam transport in ion-focused regime," *IEEE Trans. Plasma Sci.*, vol. 45, no. 12, pp. 3195–3201, Dec. 2017, doi: 10.1109/TPS.2017.2771337.

[16] M. A. Mostrom, D. Mitrovich, D. R. Welch, and M. M. Campbell, "Erosion and evaporation theory in ion-focused electron-beam transport," *Phys. Plasmas*, vol. 3, no. 9, pp. 3469–3484, Sep. 1996, doi: 10.1063/1.871497.

[17] L. Shenggang, Y. Yang, M. Jie, and D. M. Manos, "Theory of wave propagation along a waveguide filled with moving magnetized plasma," *Phys. Rev. E, Stat. Phys. Plasmas Fluids Relat. Interdiscip. Top.*, vol. 65, no. 3, Mar. 2002, Art. no. 036411, doi: 10.1103/PhysRevE.65.036411.

[18] S. B. Swanekamp, J. P. Holloway, T. Kammash, and R. M. Gilgenbach, "The theory and simulation of relativistic electron beam transport in the ion-focused regime," *Phys. Fluids B, Plasma Phys.*, vol. 4, no. 5, pp. 1332–1348, May 1992, doi: 10.1063/1.860088.

[19] C. Popovici, M. Someşan, and V. Nistor, "Beam-plasma instability in the hollow cathode discharge," *Phys. Lett.*, vol. 22, no. 5, pp. 587–588, 1966, doi: 10.1016/0031-9163(66)90667-6.

[20] P. C. de Jagher, F. W. Sluijter, and H. J. Hopman, "Relativistic electron beams and beam-plasma interaction," *Phys. Rep.*, vol. 167, no. 4, pp. 177–239, 1988, doi: 10.1016/0370-1573(88)90094-4.

[21] A. E. Dubinov, A. G. Petrik, S. A. Kurkin, N. S. Frolov, A. A. Koronovskii, and A. E. Hramov, "Beam-plasma instability in charged plasma in the absence of ions," *Phys. Plasmas*, vol. 23, no. 4, Apr. 2016, Art. no. 042105, doi: 10.1063/1.4945644.

[22] J. P. Verboncoeur, A. B. Langdon, and N. T. Gladd, "An object-oriented electromagnetic PIC code," *Comput. Phys. Commun.*, vol. 87, nos. 1–2, pp. 199–211, 1995, doi: 10.1016/0010-4655(94)00173-Y.

[23] M. Stetter, P. Felsner, J. Christiansen, K. Frank, A. Gortler, G. Hintz, T. Mehr, R. Stark, and R. Tkotz, "Investigation of the different discharge mechanisms in pseudospark discharges," *IEEE Trans. Plasma Sci.*, vol. 23, no. 3, pp. 283–293, Jun. 1995, doi: 10.1109/27.402314.

[24] T. Hisashi, T. Sato, M. Itagaki, M. Watanabe, T. Morikawa, Y. Abe, and T. Shimada, "Effects of electrode geometry on breakdown voltage of a single-gap pseudospark discharge," *Jpn. J. Appl. Phys.*, vol. 37, no. 1, pp. 303–307, 1998, doi: 10.1143/jjap.37.303.

[25] H. Yin, "Pseudospark discharge and Cherenkov maser experiments," Ph.D. dissertation, Dept. Phys., Univ. Strathclyde, Glasgow, Scotland, 1998.

[26] M. C. Wang, J. Zhu, Z. Wang, L. Zhang, Y. Huang, C. Feng, J. K. Lee, and E. H. Park, "Intense electron beam generation by a pseudospark discharge and its application to a Raman FEL," in *Proc. Int. Conf. Plasma Sci.*, Jun. 1995, p. 288, doi: 10.1109/PLASMA.1995.533543.

[27] J. Zhao, H. Yin, L. Zhang, G. Shu, W. He, A. D. R. Phelps, A. W. Cross, L. Pang, and Q. Zhang, "Study of the beam profile and position instability of a post-accelerated pseudospark-sourced electron beam," *Phys. Plasmas*, vol. 24, no. 3, Mar. 2017, Art. no. 033118, doi: 10.1063/1.4978788.

[28] C. Xu, B. Wang, R. Peng, L. Bi, F. Zeng, Z. Chang, S. Zhu, Y. Yin, H. Li, and L. Meng, "Start current study of a THz sheet beam extended interaction oscillator," *Phys. Plasmas*, vol. 25, no. 7, Jul. 2018, Art. no. 073103, doi: 10.1063/1.5027445.

LIANG ZHANG (Senior Member, IEEE) received the B.Sc. degree in applied physics from the University of Science and Technology of China, Hefei, China, in 2004, the M.Sc. degree in application of nuclear techniques from the China Academy of Engineering Physics, Chengdu, China, in 2007, and the Ph.D. degree in physics from the University of Strathclyde, Glasgow, U.K., in 2012. He is currently a Research Fellow with the Scottish Universities Physics Alliance, Department of Physics, University of Strathclyde. His main research interests include pulse-power technology, gyrotron travelling wave amplifiers/backward-wave oscillators/klystrons, microwave undulators, electron beam generation and beam-wave interactions, low-pressure gas discharges, and plasma filled high power microwave sources and free electron lasers.

ALAN D. R. PHELPS (Member, IEEE) received the B.A. degree (Hons.) in physics and the M.A. degree from Cambridge University, U.K., in 1966 and 1970, respectively, and the D.Phil. degree from Oxford University, U.K., in 1970. In 1978, he joined the University of Strathclyde, Glasgow, U.K., becoming a Professor, in 1993. His research interests include high-power free-electron radiation sources and plasmas. He is a fellow of the American Physical Society (APS), the Institute of Physics, and the Royal Society of Edinburgh. He received the IEEE Plasma Science and Applications (PSAC) Award, in 2017.

KEVIN RONALD (Member, IEEE) was born in Glasgow, U.K. He received the B.Sc. (Hons.) and Ph.D. degrees in physics from the University of Strathclyde, Glasgow, in 1992 and 1997, respectively. He is currently a Professor with the Department of Physics, University of Strathclyde, where he is affiliated with the Scottish Universities Physics Alliance (SUPA). His research interests include low-temperature plasmas, beam plasma and wave plasma interactions, geophysical plasma electrodynamics, microwave amplifiers and oscillators, and muon ionization cooling. He is a member of the Institute of Physics (IoP), the European Physical Society (EPS), and the American Physical Society (APS).

ADRIAN W. CROSS (Member, IEEE) received the B.Sc. degree (Hons.) in physics and the Ph.D. degree from the University of Strathclyde, Glasgow, U.K., in 1989 and 1993, respectively. He joined the ABP Group, University of Strathclyde, in 1993, initially as a Research Fellow, and then as a Lecturer, in 2000, a Senior Lecturer, in 2005, and a Reader, in 2007, with the Department of Physics. He is currently a Professor with the Atoms, Beams and Plasmas Group (ABP), Department of Physics, University of Strathclyde. From 2002 to 2007, he was an Engineering and Physical Science (EPSRC) Advanced Fellow. He has been involved in various aspects of research on gyrotrons, cyclotron autoresonance masers, free-electron lasers, superradiant sources, gyrotron travelling wave amplifiers, and plasma applications. More recently, he has primarily been concentrating on THz radiation sources and pseudospark discharge physics. He is a member of the Institute of Physics (IoP).

• • •